Forearc carbon sequestration reduces long-term volatile recycling into the mantle

P.H. Barry[1,2,3]*, J. M. de Moor[4,5],‡ D. Giovannelli[6,7,8,9],‡ M. Schrenk[10], D. Hummer[11], T. Lopez[12], C.A. Pratt[13],Y. Alpízar Segura[14], A. Battaglia[15], P. Beaudry[16], G. Bini[17], M. Cascante[4], G. d'Errico[6,18], M. di Carlo[18], D. Fattorini[18,19], K. Fullerton[20], E. Gazel[21], G. González[14], S. A. Halldórsson[22], K. Iacovino[23,24], J.T. Kulongoski[2,25], E. Manini[6], M. Martínez[4], H. Miller[10], M. Nakagawa[8], S. Ono[16], S. Patwardhan[7], C.J. Ramírez[14], F. Regoli[18,19], F. Smedile[7], S. Turner[26], C. Vetriani[7], M. Yücel[27], C.J. Ballentine[1], T.P. Fischer[5], D.R. Hilton[25], K.G. Lloyd[20‡]

[1]Department of Earth Sciences, University of Oxford, UK

[2]USGS, California Water Science Center, CA, USA

[3]Now at: Marine Chemistry and Geochemistry Department, Woods Hole Oceanographic Institution, Woods Hole, MA, USA

*Correspondence email: pbarry@whoi.edu

[4]Observatorio Volcanológico y Sismológico de Costa Rica (OVSICORI), Universidad Nacional, Costa Rica

[5]Department of Earth and Planetary Sciences, University of New Mexico, NM, USA

[6]Institute of Institute for Marine Biological and Biotechnological Resources, National Research Council of Italy, (IRBIM-CNR), Ancona, Italy

[7]Department of Marine and Coastal Science, Rutgers University, New Brunswick, NJ, USA

[8]Earth-Life Science Institute, Tokyo Institute for Technology, Tokyo, Japan

[9]Now at: Department of Biology, University of Naples "Federico II", Naples, Italy

[10]Michigan State University, MI, USA

[11]Southern Illinois University, IL, USA

[12]University of Alaska, Fairbanks, AK, USA

[13]University of Rhode Island, RI, USA

[14]Volcanes Sin Fronteras (VSF), Costa Rica

[15]Università degli Studi di Palermo, Palermo, Italy

[16]Massachussetts Institute of Technology, MA, USA
[17]Univesity of Florence, Italy
[18]Dipartimento di Scienze della Vita e dell'Ambiente (DISVA), Università Politecnica delle Marche (UNIVPM), Italy
[19]CoNISMa, Consorzio Nazionale Interuniversitario Scienze del Mare, Italy
[20]University of Tennessee, TN, USA
[21]Department of Earth and Atmospheric Sciences, Cornell University, NY, USA
[22]NordVulk, Institute of Earth Sciences, University of Iceland, Iceland
[23]Arizona State University, AZ, USA
[24]Now at: Johnson Space Center, NASA, TX, USA
[25]Scripps Institution of Oceanography, University of California, CA, USA
[26]Washington University in St Louis, St. Louis, MO, USA
[27]Institute of Marine Sciences, Middle East Technical University, Erdemli, Turkey
‡ Equally contributing authors

Nature

Number of Words in Summary= 150

Number of Words in Main Text = 3,114

Number of Figures = 4

Extended data Figures = 3

Number of Tables = 0

Number of Supplementary Tables = 4

Main Text References = 50

Methods References = 48

Summary:

Carbon and other volatiles are transported from Earth's surface into the mantle at subduction margins. The efficiency of this transfer has profound implications for the nature and scale of geochemical heterogeneities in Earth's deep (mantle) and shallow (crustal) reservoirs, as well as Earth's oxidation state. However, the proportion of volatiles released in the forearc and backarc are not well-constrained compared to fluxes from the volcanic-front. Here, we use helium and carbon isotope data from deeply-sourced springs along two cross-arc transects to show that ~91% of carbon released from the slab/mantle beneath the Costa Rica forearc is sequestered within the crust by calcite deposition, and an additional ~3% is incorporated into biomass through microbial chemolithoautotrophy. We estimate that ~1.2×10^8 to 1.3×10^{10} mol CO_2/yr are released from the slab beneath the forearc, resulting in up to ~19% less carbon being transferred to Earth's deep mantle than previously estimated.

Main Text:

Terrestrial carbon traverses various reservoirs on Earth from the surface to the mantle. It is subjected to a number of geological, geochemical, and biological cycles, each of which operates on vastly different temporal and spatial scales. Perhaps the most important physical process linking the deep and shallow carbon cycles is subduction, which transports both oxidized and reduced forms of crustal carbon into the mantle. During subduction, volatile-rich fluids are released from the downgoing slab (upper mantle and crust). These fluids are thought to migrate through the overlying mantle-wedge and crust, and are ultimately released across the forearc, volcanic arc-front and backarc (i.e., behind the volcanic front). However, little is known about what effect volatile fluxes through the forearc may have on the total volatile budget and estimates of recycling efficiency[1]. Much of the forearc subsurface is at low temperatures (<100°C) that are conducive to microbial life as well as shallow water-rock interactions. Therefore,

83 microorganisms and/or abiotic chemical processes may alter the speciation, isotopic
84 composition, and presumed carbon budgets. Regional-scale effects of these shallow
85 processes on volatile fluxes in the forearc have not previously been quantified.
86
87 Carbon budgets for convergent margins typically assume negligible carbon
88 emissions from the area between the trench (i.e., where the downgoing slab subducts
89 beneath the overriding plate) and the degassing volcanic arc-front[1-3]. It is not clear
90 whether the lack of obvious high emission sources reflects a lack of deep CO_2 input from
91 the slab-mantle mixture, or if secondary processes in the upper plate[4-5] mask diffuse but
92 significant CO_2 release.
93
94 Carbon outputs at the Central American Volcanic Arc, which have been the focus
95 of several studies, are estimated to represent only 12% of the total subducted carbon
96 input along the middle American trench[2,6-7], whereas global arcs typically have carbon
97 outputs that approach their inputs, suggesting limited volatile delivery to the mantle[1].
98 However, recent work[8] proposed a far higher volcanic carbon flux for Central America,
99 suggesting that this region may be more similar to other arc segments[1] than previously
100 thought[2,6]. Our study focuses on the Nicoya Peninsula area of Costa Rica in part because it
101 is one of the few places on Earth with easy sampling access to an on-land forearc region
102 and thus presents an opportunity to study the fate of carbon across an entire arc. Few
103 carbon flux estimates have been made from the forearc region of any arc, despite the fact
104 that there is plentiful ancillary evidence for fluid venting in forearc regions (*e.g.,*
105 serpentinite diapirism in the Marianas[9] and mud volcanism at various accretionary prisms
106 worldwide[10]), as well as ample geophysical evidence that shows fluid upwelling in the
107 forearc region from the downgoing slab[11]. In Costa Rica, the only available forearc data
108 are from three submarine venting sites[3], where the authors estimated that the carbon
109 output from the outer forearc represents less than 1% of the carbon input at the trench.
110 Taking into account the loss at the volcanic-front, they proposed two explanations: either
111 subducted carbon was largely transported into the deep mantle or significant quantities

of carbon were lost to the forearc or backarc regions. Independently, thermodynamic models of subduction predict significant CO_2 loss (i.e., decarbonation) from the top of the subducting slab beneath global forearc regions[12], as the slab penetrates to greater temperature and pressure conditions.

The extensive occurrence of calcite veining throughout the Costa Rica forearc[13-14] suggests that much of the CO_2 released from the slab beneath the forearc could be sequestered into the crust as calcite, in which case direct measurements of diffuse degassing in this region are not representative of deep mantle processes. Additional mechanisms for masking CO_2 gas release in the upper plate include microbial biomass production, conversion to CH_4, trapping in reservoirs beneath impermeable caps, and abiotic organic matter synthesis. Calcite deposition results in a temperature dependent isotope fractionation and may be microbially mediated[15-16] in cation-rich alkaline waters with high aqueous CO_2 concentrations. Additionally, in the absence of light for photosynthesis, microorganisms in subsurface settings instead fix CO_2 into biomass through chemolithoautotrophy[17-19]. Both calcite deposition and chemolithoautotrophy occur mostly at temperatures below 100°C, which are the prevalent conditions in the forearc subsurface[20]. Biologically induced carbon fixation generally results in a kinetic fractionation of carbon isotopes that preferentially removes ^{12}C from CO_2[21]. The degree of fractionation depends on the microorganism's physiology, as well as substrate limitations, temperature, and pressure. Biological activity can also decrease the carbon isotopic composition ($\delta^{13}C$) of CO_2, by adding ^{13}C-depleted carbon through heterotrophic respiration of organic matter or methane. This process is not associated with a large carbon isotope fractionation[21] relative to pure kinetic reactions driven solely by biological processes. In addition, abiotic hydrocarbon production from dissolved CO_2 has been demonstrated in laboratory experiments over 250°C[22], a possible temperature regime in hotter forearc regions.

He and C Results:

We collected samples from 23 sites in northern and central Costa Rica (Figure 1), which traversed forearc (Nicoya Peninsula), arc and backarc regions. Springs likely to represent deeply-sourced fluids (based on field data such as temperature, dissolved oxygen, salinity) were targeted, and samples were taken by inserting tubes into outflow vents to minimize fluid interaction with atmosphere and surface water. The sites were classified into two groups: the northern transect samples, which were collected to the north of the EPR-CNS on-land extension, and the Central transect samples, which were collected to the south of this plate transition. The two groups, with the exception of Santa Lucia, are separated by the on-land extension of a major transition in the downgoing slab: the boundary between oceanic crust formed at the East Pacific Rise (EPR) and the Cocos Nazca Spreading (CNS) zone. We measured $^{3}He/^{4}He$ vs. air, expressed as (R/R_A), where $R = {}^{3}He/{}^{4}He_{sample}$ and $R_A = {}^{3}He/{}^{4}He_{air}=1.39 \times 10^{-6}$ for 17 geothermal fluid (i.e., spring water) samples and 17 free gas samples. In addition, we measured $\delta^{13}C$ vs. Vienna Pee Dee Belemnite (VPDB) in dissolved inorganic carbon (DIC) in 31 geothermal fluid samples, dissolved organic carbon (DOC) in 16 fluid samples, and CO_2 in 16 free gas samples (Supplementary Table 1). Sediments surrounding the surface emanation of the springs were also sampled and total organic carbon (TOC) contents and $\delta^{13}C$ were measured. The relative abundances of He to CO_2 are also reported ($CO_2/^{3}He$; Extended Data Figure 1). The air-normalized $^{4}He/^{20}Ne$ ratio is used to calculate the X-value, (multiplied by the Bunsen solubility (1.23) at the assumed recharge temperature of 15°C[23] for fluid samples), which is used to estimate the air-corrected $^{3}He/^{4}He$ ratio (R_C) of the sample[24]. As X-values are high (>5) for the majority of samples of this study (Extended Data Figure 2), the correction factor is small and hence there is typically little difference between measured (R/R_A) and corrected (R_C/R_A) $^{3}He/^{4}He$ ratios (Supplementary Table 1).

The air-corrected $^{3}He/^{4}He$ (R_C/R_A) values range from 0.49 to 6.79 R_A (Supplementary Table 1), with the highest values occurring in the volcanic arc and the lowest occurring in the outer forearc. Arc values approach upper mantle values (~ 8 R_A),

however, they exhibit evidence for a small but discernible addition of radiogenic helium at all locations. In contrast, outer forearc and forearc values are predominantly radiogenic, with a small but distinct mantle contribution, suggesting these fluids are an admixture of crustal fluids and deeply sourced volatiles likely with some influence of shallow water-rock interaction. He-isotope values are systematically higher (i.e., more mantle-like) in both fluids and gases close to the volcanic arc-front and lower toward the trench (i.e., in the forearc; Figure 2A), showing that slab/mantle outgassing is not limited to the arc-front, and occurs throughout the entire forearc. However, free CO_2 gas (bubbling springs) was only detected within ~20km of the arc (Figure 2B). In the absence of gas manifestations, we examined evidence for forearc carbon processing in dissolved carbon from spring outflows.

The $\delta^{13}C$ and carbon content of DIC and DOC within spring fluids decrease systematically trenchward across the entire arc (Figure 2B and Figure 3). Strikingly, DIC values in northern and central Costa Rica follow distinct parallel trends (Figure 3), which are not masked by site-dependent surface-derived organic material heterogeneities, such as vegetation, degradation of photosynthetic organic matter and/or surface water infiltration, indicating that the distribution of carbon in these fluids results from deep subsurface phenomena. In contrast, TOC is heavily influenced by surface detrital carbon and shows no apparent trend between concentration and $\delta^{13}C$ in samples across the two transects. DIC and DOC define Rayleigh distillation curves, with northern springs showing consistently higher $\delta^{13}C$ for both DIC and DOC at a given DIC content. The parallel trends of decreasing $\delta^{13}C$ with decreasing DIC are consistent with isothermal (~65°C) precipitation of isotopically heavy calcite from forearc fluids (see methods for details), with generally higher degrees of calcite precipitation observed closer to the trench. This model is supported by water chemistry data; PhreeqC was used to show that all outer forearc samples are strongly saturated with respect to calcite and thus would be predicted to readily precipitate calcite (Supplementary Table 3). We present a model for calcite

199 precipitation that closely fits the observed data distribution (Figure 3), but requires a
200 more positive $\delta^{13}C$ value of the deep total dissolved carbon (DC = DIC+DOC) source
201 fluid (+5.0‰) released from the slab in northern Costa Rica than in central Costa Rica
202 (+0.5‰). Volcanic gases, which are presumed to represent the primary magmatic
203 fluid, show isotopically more negative values than dissolved carbon in the calculated
204 DIC endmember fluids, due to the additional isotopic fractionation associated with
205 dissolution of CO_2 gas into an aqueous fluid[25] (Figure 3). Importantly, the modeled
206 initial dissolved carbon values thus reflect both the isotopic composition of the
207 subduction fluids and a fractionation effect derived from CO_2 dissolution from source
208 gases[26-27] (Figure 3). Our data suggest that surface carbon expressions across the
209 forearc are ultimately inherited from slab/mantle fluids, which are intricately linked
210 to the tectonics of the region, and modified by broadly coherent shallow processes.
211
212 **Origin of fluids:**
213 The observation that northern and central Costa Rica samples have markedly
214 different source fluid compositions suggests a relationship to the character of the
215 subducting slab. The northern EPR crust has a higher density of seamounts and is
216 more permeable than the CNS crust[28]. The higher resulting fluid flow through sub-
217 seafloor basalts at the EPR cools, hydrates, and chemically weathers the plate[29].
218 Building on previous models[30], we hypothesize that the higher fluid flow from this
219 water-rich downgoing slab flushes more carbon from the slab upward into the
220 overriding plate at shallower depths beneath the forearc, accounting for the greater
221 contributions of relatively ^{13}C-enriched carbonates in our northern sample set.
222 Additionally, enhanced fluid circulation in the EPR crust likely promotes calcite
223 veining in the downgoing plate, potentially providing an additional source of heavy
224 carbon[31] in northern Costa Rica. Thus, the composition of the subducting slab is
225 expressed in surface-manifestations across the forearc. Our model predicts that
226 source fluids from northern Costa Rica are more ^{13}C-enriched than in central Costa
227 Rica (Figure 3). Both volcanic arc CO_2 and dissolved forearc carbon reflect a larger

carbonate contribution in northern Costa Rica, which is consistent with previous observations in the volcanic arc which show an increased carbonate signal in northern Costa Rica, which extends into Nicaragua[30, 32-36].

Importantly, the carbon isotope compositions of forearc springs can be used to calculate the fraction of carbon lost through calcite deposition (see Figure 3 and methods for details). Using the average $\delta^{13}C$ of the DC ($\delta^{13}C_{DC}$) of all the forearc springs for each transect (northern = -8.8‰, central = -14.3‰) we find that 88% and 89% of the total carbon released in the forearc is precipitated as calcite, respectively. Using the average $\delta^{13}C_{DC}$ of the outer forearc springs (i.e., Nicoya Peninsula only; northern = -14.4‰, central = -16.5‰) yields 95% and 92% of the total carbon precipitated as calcite, for the northern and central transects, respectively. The close agreement between the calculated fractions of total carbon lost to calcite is due to the fact that the Rayleigh fractionation curves are steep at low $\delta^{13}C$ values (Figure 3). Thus, a large range in $\delta^{13}C$ observed in the forearc corresponds to a relatively narrow range of calculated fractionation (F) values (i.e., fraction of carbon remaining; Figure 3). We conclude that 91 ± 4% of forearc carbon is lost through calcite precipitation.

Measured DOC $\delta^{13}C$ values varied widely from -0.65 to -25.48‰ vs. VPDB, with a mean value of -12.00‰. Like DIC, the lowest values were observed in the outer forearc and the highest values were observed in the forearc, where values are highly variable (Figure 2B and 2C). However, with the exception of one site in the central region (Santa Lucia), DOC carbon isotope compositions and concentrations strongly correlate with those of DIC (Figure 3), suggesting that DOC is produced from deeply sourced fluids. Considering this, we propose a two-stage model whereby 91 ± 4% of the carbon released from the slab/mantle is consumed by calcite precipitation and the remaining dissolved carbon is further fractionated by biological consumption. Our model assumes a steady-state flux of deep (slab/mantle) fluids, which imparts the carbon isotope signature of the slab into the upper plate where carbon is

partitioned into CO_2 gas, calcite, DIC, and DOC. DOC is potentially a mixture of deep thermogenic DOC, deep microbial chemolithoautotrophy, and shallow photosynthetic DOC. The outlier DOC sample, Santa Lucia, is likely dominated by deep thermogenic DOC, due to the fact that it has an anomalously high DOC concentration (5.69mmolC/L), $\delta^{13}C$ value (-0.65‰), and polycyclic aromatic hydrocarbon concentrations (Supplementary Table 2), accompanied by a pronounced visible oily sheen on the surface fluids. In all other sampling sites, DOC is likely synthesized from DIC at physiologically feasible temperatures in the subsurface rather than being a mixture of exogenous sources, since its concentrations and $\delta^{13}C$ values correlate tightly with DIC.

DIC and DOC carbon isotopes are offset from each other by 10.9 ± 1.6‰ in the north, and 5.8 ± 2.2‰ in the central region (Figure 3); these $\Delta^{13}C_{DIC\text{-}DOC}$ values are within the expected range for the reverse tricarboxylic cycle, which is a common microbial carbon fixation pathway in the subsurface[17,37]. The $\Delta^{13}C_{DIC\text{-}DOC}$ values are also consistent with isotopic fractionation of hydrocarbons synthesized abiotically from DIC at 250°C[22]. However, calcite precipitation occurs at ~65°C, and DOC synthesis must occur after calcite precipitation for DOC carbon isotope compositions to correlate with the post-precipitation DIC values. Therefore most of the DOC appears to be derived from subsurface chemolithoautotrophy at <65°C. This is further supported by the detection of microbial cells in all hot spring fluids except Las Hornillas. We conclude that DOC at the remaining sites is primarily synthesized from chemolithoautotrophy within the deep subsurface environment and that slab/mantle-derived carbon is used by microorganisms to build biomass. By using cell abundance values for the sampled subsurface fluids, we estimate that up to 2.8×10^9 moles of additional carbon could be locked into biomass in the Costa Rican forearc, potentially contributing significantly to the overall carbon sink.

These findings have major implications for the global carbon mass balance of subduction zones. We calculate a CO_2 flux from the forearc (Supplementary Table 4) by combining the average DIC concentration in forearc waters of 4.24 mmol/L CO_2 with measured flow rates, which ranged between 1-10 L/s and an estimated 50-500 springs[38] throughout the forearc region. We further consider that 5-50 of these springs have a separate gas phase, with measured CO_2 fluxes of 201 mol × m^{-2} × d^{-1} to 655 mol × m^{-2} × d^{-1}, and bubbling areas that typically cover 1 m^2 to 10 m^2 based on our field observations. Using these broad criteria, the steady-state CO_2 flux is constrained to 7.1 × 10^6 to 7.9 × 10^8mol/yr (mean = 4.0 × 10^8), which is two orders-of-magnitude smaller than the volcanic-arc flux (1.3-6.1× 10^{10} mol/yr)[2,8]. As argued above, carbon isotopes indicate that forearc calcite deposition and chemolithoautotrophy together remove ~94% of the total carbon inputs. This increases the flux range that we calculate to 1.2 × 10^8 to 1.3 × 10^{10} mol/yr, which is significantly larger than the previous outer forearc estimate of 2.1 × 10^7 mol/yr, determined using a smaller number of submarine seeps[3]. This represents up to 36% of the total volcanic-arc flux (= 3.7 × 10^{10} ± 66% mol/yr; taken as the mean of previous CO_2 flux estimates from references[2,8]; Figure 4; Supplementary Table 4), which would result in a ~19% reduction in the amount of total carbon transported to the deep mantle. Similarly, dissolved CH_4 concentrations and CH_4/CO_2 in sampled fluids are used to constrain the CH_4 flux from 5.1 × 10^3 to 1.0 × 10^6mol/yr. Thus, CH_4 emissions contribute negligibly to the total forearc C budget.

Implications for evolution of Earth Reservoirs:

Our results suggest that significantly less carbon is transported into Earth's mantle than previous estimates suggest[1], due to the previously unrecognized calcite forearc carbon sink. This observation has wide ranging implications for the volatile inventory of the mantle and the temporal evolution of Earth reservoirs, which controls the planet's redox balance[39-41]. For example, the nature (reduced vs. oxidized carbon) and extent of carbon reaching the mantle is intricately linked to volatile recycling, and impacts the net oxidation state of Earth's surface and deep interior. Furthermore, we

propose that carbon sequestration in the forearc may be directly related to plate subduction angle, which dictates the extent of forearc. Globally, flat subduction zones represent only about 10% of total subduction zones[42], which would indicate that approximately 2% less carbon than previously estimated is currently delivered to the deep mantle. However, such a carbon sink may have been enhanced during the late Archean, when oceanic crust was subducted at an anomalously low-angle[43]. Notably, evidence for the so-called Archean flat-subduction is preserved in most late Archean (3.0–2.5 Ga) terrains, but is lacking in the early Archean (>3.3 Ga). If carbon was stored overwhelmingly on continental (or island arc) margins, then continental collisions and continental arc flare-ups would be the most important regulator of atmospheric CO_2 through time. During the Proterozoic, subduction zones were dominated by high dip angles and smaller forearcs[44], enabling volatiles to be more efficiently transferred into deep mantle, as the forearc carbon sink would likely be less significant and transfer to the mantle would be more efficient. A more efficient transfer of reduced carbon to the mantle could then lead to enhanced accumulation of oxygen in the atmosphere over time. Thus, this work provides potential forcing mechanisms on the great oxygenation event, which was certainly controlled in part by subduction efficiency and plate tectonics[45-47]. In addition, these findings also have implications for the modern atmosphere, as better constraints on the long-term volcanic carbon budget and how it may be buffered by chemical and biological processes is critical for evaluating natural and anthropogenic climate forcings.

Main Text References:

1. Kelemen, P. B., & Manning, C. E. Reevaluating carbon fluxes in subduction zones, what goes down, mostly comes up. *Proceedings of the National Academy of Sciences*, 112(30), E3997-E4006. (2015).

2. Shaw, A. M., Hilton, D. R., Fischer, T. P., Walker, J. A., & Alvarado, G. E. Contrasting He–C relationships in Nicaragua and Costa Rica: insights into C cycling through subduction zones. *Earth and Planetary Science Letters*, 214(3-4), 499-513. (2003).

3. Füri, E., Hilton, D. R., Tryon, M. D., Brown, K. M., McMurtry, G. M., Brückmann, W., & Wheat, C. G. Carbon release from submarine seeps at the Costa Rica fore arc: Implications for the volatile cycle at the Central America convergent margin. *Geochemistry, Geophysics, Geosystems*, 11(4). (2010).

4. Schwarzenbach, E.M., Früh-Green, G.L., Bernasconi, S.M., Alt, J.C. and Plas, A. Serpentinization and carbon sequestration: A study of two ancient peridotite-hosted hydrothermal systems. *Chemical Geology*, 351, pp.115-133. (2013).

5. McCollom, T. M., & Seewald, J. S. Serpentinites, hydrogen, and life. *Elements*, 9(2), 129-134. (2013).

6. Hilton, D. R., Fischer, T. P., & Marty, B. Noble gases and volatile recycling at subduction zones. *Reviews in mineralogy and geochemistry*, 47(1), 319-370. (2002).

7. de Leeuw, G.A.M., Hilton, D.R., Fischer, T.P. and Walker J.A., The He-CO_2 isotope and relative abundance characteristics of geothermal fluids in El Salvador and Honduras: New constraints on volatile mass balance of the Central American Volcanic Arc, *Earth and Planetary Science Letters*, 258(1–2), 132–146. (2007).

8. de Moor, J.M., Kern, C., Avard, G., Muller, C., Aiuppa, A., Saballos, A., Ibarra, M., LaFemina, P., Protti, M. and Fischer, T.P.. A new sulfur and carbon degassing inventory for the Southern Central American Volcanic Arc: The importance of accurate time-series data sets and possible tectonic processes responsible for temporal variations in arc-scale volatile emissions. *Geochemistry, Geophysics, Geosystems*, 18(12), pp.4437-4468. (2017).

9. Fryer, P., Ambos, E. L., & Hussong, D. M. Origin and emplacement of Mariana forearc seamounts. *Geology*, 13(11), 774-777. (1985).

10. Brown, K. M. The nature and hydrogeologic significance of mud diapirs and diatremes for accretionary systems. *Journal of Geophysical Research: Solid Earth*, 95(B6), 8969-8982. . (1990).

11. Naif, S., Key, K., Constable, S., & Evans, R. L. Water-rich bending faults at the Middle America Trench. *Geochemistry, Geophysics, Geosystems*, 16(8), 2582-2597. (2015).

12. Gorman, P. J., Kerrick, D. M., & Connolly, J. A. D. Modeling open system metamorphic decarbonation of subducting slabs. *Geochemistry, Geophysics, Geosystems*, 7(4). (2006).

13. Vaca, L., Alvarado, A., & Corrales, R. Calcite deposition at Miravalles geothermal field Costa Rica. *Geothermics*, 18(1-2), 305-312. (1989).

14. Corrigan, J., Mann, P., & Ingle Jr, J. C. Forearc response to subduction of the Cocos ridge, Panama-Costa Rica. *Geological Society of America Bulletin*, 102(5), 628-652. (1990).

15. Pacton, M., Wacey, D., Corinaldesi, C., Tangherlini, M., Kilburn, M.R., Gorin, G.E., Danovaro, R. and Vasconcelos, C. Viruses as new agents of organomineralization in the geological record. *Nature communications*, 5, p.4298. (2014).

16. Zhu, T. & Dittrich, M. Carbonate precipitation through microbial activities in natural environment, and their potential in biotechnology: A review. *Frontiers in Bioengineering and Biotechnology*, 4:4. (2016).

17. Berg, I. A. Ecological aspects of the distribution of different autotrophic CO_2 Fixation Pathways. *Appl. Environ. Microbiol*. 77, 1925–1936. (2011).

18. Colwell, F. S., D'Hondt, S. Nature and extent of the deep biosphere. *Reviews in Mineralogy and Geochemistry*, 75, 547-574. (2013).

19. Emerson, J. B., Thomas, B. C., Alvarez, W., & Banfield, J. F. Metagenomic analysis of a high carbon dioxide subsurface microbial community populated by chemolithoautotrophs and bacteria and archaea from candidate phyla. *Environmental Microbiology*, 18(6), 1686-1703. (2016).

20. Harris, R. N., & Wang, K. Thermal models of the middle America trench at the Nicoya Peninsula, Costa Rica. *Geophysical Research Letters*, 29(21), 6-1. (2002).

21. Whiticar, M. J. Carbon and hydrogen isotope systematics of bacterial formation and oxidation of methane. *Chemical Geology*, 161(1-3), 291-314. (1999).

22. McCollom, T. M., & Seewald, J. S. Abiotic synthesis of organic compounds in deep-sea hydrothermal environments. *Chemical Reviews*, 107(2), 382-401. (2007).

23. Ozima, M., & Podosek, F. A. Noble gas geochemistry. *Cambridge University Press*. (2002).

24. Hilton, D. R. The helium and carbon isotope systematics of a continental geothermal system: results from monitoring studies at Long Valley caldera (California, USA). *Chemical Geology*, 127(4), 269-295. (1996).

25. Mook, W.G., Bommerson, J.C., Stavermann, W.H. Carbon isotope fractionation between dissolved bicarbonate and gaseous carbon dioxide. Earth and Planetary Science Letters 22, 169 (1974).

26. Vogel, J. C., Grootes, P. M., &Mook, W. G. Isotopic fractionation between gaseous and dissolved carbon dioxide. *ZeitschriftfürPhysik A Hadrons and nuclei*, 230(3), 225-238. (1970).

27. Barry, P. H., Hilton, D. R., Fischer, T. P., De Moor, J. M., Mangasini, F., & Ramirez, C. Helium and carbon isotope systematics of cold “mazuku” CO2 vents and hydrothermal gases and fluids from Rungwe Volcanic Province, southern Tanzania. *Chemical Geology*, 339, 141-156. (2013).

28. Audet, P., & Schwartz, S. Y. Hydrologic control of forearc strength and seismicity in the Costa Rican subduction zone. *Nature Geoscience*, 6(10), 852. (2013).

29. Wheat, C. G., & Fisher, A. T. Massive, low-temperature hydrothermal flow from a basaltic outcrop on 23 Ma seafloor of the Cocos Plate: Chemical constraints and implications. *Geochemistry, Geophysics, Geosystems*, 9(12). (2008).

30. Aiuppa, A., Robidoux, P., Tamburello, G., Conde, V., Galle, B., Avard, G., Bagnato, E., de Moor, J.M., Martinez, M., Muñoz, A. Gas measurements from the Costa Rica-Nicaragua volcanic segment suggest possible along-arc variations in volcanic gas chemistry. *Earth and Planetary Science Letters*, 407, 134-147. (2014).

31. Alt J. C., Laverne C., Coggon R. M., Teagle D. A., Banerjee N. R., Morgan S., Smith-Duque C. E., Harris M., & Galli L. Subsurface structure of a submarine hydrothermal system in ocean crust formed at the East Pacific Rise, ODP/IODP Site 1256. *Geochemistry, Geophysics, Geosystems*, 11(10). (2010).

32. Carr, M. J., Feigenson, M. D., & Bennett, E. A. Incompatible element and isotopic evidence for tectonic control of source mixing and melt extraction along the Central American arc. *Contributions to Mineralogy and Petrology*, 105(4), 369-380. (1990).

33. Leeman, W. P., Carr, M. J., & Morris, J. D. Boron geochemistry of the Central American volcanic arc: constraints on the genesis of subduction-related magmas. *Geochimica et Cosmochimica Acta*, 58(1), 149-168. (1994).

34. Zimmer, M. M., Fischer, T. P., Hilton, D. R., Alvarado, G. E., Sharp, Z. D., & Walker, J. A. Nitrogen systematics and gas fluxes of subduction zones:

insights from Costa Rica arc volatiles. *Geochemistry, Geophysics, Geosystems*, 5(5). (2004).

35. Hilton, D. R., Ramirez, C. J., Mora-Amador, R., Fischer, T. P., Füri, E., Barry, P. H., & Shaw, A. M. Monitoring of temporal and spatial variations in fumarole helium and carbon dioxide characteristics at Poás and Turrialba volcanoes, Costa Rica (2001-2009). *Geochemical Journal*, 44(5), 431-440. (2010).

36. Lee, H., Fischer, T. P., de Moor, J. M., Sharp, Z. D., Takahata, N., & Sano, Y. Nitrogen recycling at the Costa Rican subduction zone: The role of incoming plate structure. *Scientific Reports*, 7(1), 13933. (2017).

37. House, C. H., Schopf, J. W., & Stetter, K. O. Carbon isotopic fractionation by Archaeans and other thermophilic prokaryotes. *Organic Geochemistry*, 34(3), 345-356. (2003).

38. Alvarado, G.E. & Vargas, A.G., History of discovery and exploitation of thermal water in Costa Rica. *Revista Geológica de América Central*, (57), pp.55-84 (2017).

39. Marty, B., & Dauphas, N. The nitrogen record of crust–mantle interaction and mantle convection from Archean to present. *Earth and Planetary Science Letters*, 206(3), 397-410. (2003).

40. Hirschmann, M. M., & Dasgupta, R. The H/C ratios of Earth's near-surface and deep reservoirs, and consequences for deep Earth volatile cycles. *Chemical Geology*, 262(1-2), 4-16. (2009).

41. Jelen, B. I., Giovannelli, D., and Falkowski, P. G. The Role of Microbial Electron Transfer in the Coevolution of the Biosphere and Geosphere. Annual Review of Microbiology 70, 45–62. (2016).

42. Li, Z.H., Xu, Z.Q., Gerya, T.V. Flat versus steep subduction: Contrasting modes for the formation and exhumation of high- to ultrahigh-pressure rocks in continental collision zones. *Earth and Planetary Science Letters*, 301 (1-2), 65-77 (2011).

43. Smithies, R. H., Champion, D. C., & Cassidy, K. F. Formation of Earth's early Archean continental crust. *Precambrian Research*, 127(1-3), 89-101. (2003).

44. Abbott, D., Drury, R., & Smith, W. H. Flat to steep transition in subduction style. *Geology*, 22(10), 937-940. (1994).

45. Holland, H. D. Volcanic gases, black smokers, and the Great Oxidation Event. *Geochimica et Cosmochimica Acta*, 66(21), 3811-3826. (2002).

46. Kump, L. R., Kasting, J. F., & Barley, M. E. Rise of atmospheric oxygen and the "upside-down" Archean mantle. *Geochemistry, Geophysics, Geosystems*, 2(1). (2001).

47. Och, L. M., & Shields-Zhou, G. A. The Neoproterozoic oxygenation event: Environmental perturbations and biogeochemical cycling. *Earth-Science Reviews*, 110(1-4), 26-57. (2012).

48. Bird, P. "An updated digital model of plate boundaries." *Geochemistry, Geophysics, Geosystems* 4.3 (2003).

49. Protti, M., Gu, F., & McNally, K. The geometry of the Wadati-Benioff zone under southern Central America and its tectonic significance: Results from a high-resolution local seismographic network. *Physics of the Earth and Planetary Interiors*, 84(1-4), 271-287. (1994).

50. Ryan, W.B.F., Carbotte, S.M. Coplan, J.O. O'Hara, S. Melkonian, A. Arko, R. Weissel, R.A. Ferrini, V. Goodwillie, A. Nitsche, F. Bonczkowski, J. & Zemsky R. Global Multi-Resolution Topography synthesis, *Geochem. Geophys. Geosyst.*, 10, Q03014. (2009).

Acknowledgments:

This project was inspired by the late Dave Hilton, who was a great mentor and friend to several of the coauthors. This work was principally supported by a grant (G-2016-7206) from the Alfred P. Sloan Foundation and the Deep Carbon Observatory to P.H.B., K.G.L., D.G., K.P., T.L., J.M.dM. and D.H. In addition, P.H.B. was supported by NSF grant 1144559 during a portion of this project. D.G. was supported by an NSF grant (MCB 15–17567) and an ELSI Origins Network (EON) research Fellowship, which is supported by a grant from the John Templeton Foundation. The opinions expressed in this publication are those of the authors and do not necessarily reflect the views of the John Templeton Foundation. This work was further supported in party by JSPS KAKENHI grants (JP17K14412, JP17H06105, JP17H02989) awarded to M.N., NSF OCE-1431598 and NASA Exobiology NNX16AL59G awarded to K.G.L., NSF grants 0206113, 0711533 and 1049713 awarded to T.P.F., and NSF grants 0003628 and 1049748 to D.R.H. M.Y. was supported by a DEKOSIM grant (BAP-08-11-DPT.2012K120880), financed by the Ministry of Development of Turkey. M.N. produced most data, and we thank her for her significant contributions. We thank Patricia Barcala Dominguez for assistance with figure illustration. We thank Bruce Deck, Marten Wahlen and Keith Blackmon for analytical assistance at SIO. We thank Bernard Marty, Guillermo

573 Alvarado, Michael Broadly, David Byrne, David Bekaert, Jabrane Libidi and Jon Wade
574 for discussions about the project.
575
576 **Author contributions:**
577 P.H.B. originally conceived the idea for the project, was lead-PI on the Sloan (Deep
578 Carbon Observatory) grant that supported the work, and prepared the first draft of
579 the manuscript. J.M.dM., D.G., and K.G.L. were all co-PIs on the grant and
580 contributed immensely (and equally) to modeling these data and to the writing
581 process. M.S. contributed significantly to modeling and writing, although he was not
582 a co-PI on the Sloan grant. D.H., T.L. and C.A.P. were co-PIs on the Sloan grant and
583 contributed to the writing process. Noble gas analysis was conducted in the
584 laboratory of C.J.B. at Oxford. T.P.F. and D.R.H. are senior PIs who first brought P.H.B.
585 and J.M.dM. to Costa Rica as PhD students, and were instrumental in the conception
586 of this project. In addition, a portion of the data reported in this contribution was
587 generated from those early expeditions. All other authors (listed alphabetically)
588 provided comments on the manuscript and either assisted in sample collection (as
589 part of the Biology Meets Subduction team or on previous expeditions) and/or
590 analyzed samples in their respective laboratories.
591
592 **Author information:**
593 The authors declare no competing interests. Reprints and permissions information is
594 available at www.nature.com/reprints. Correspondence and requests for materials
595 should be addressed to pbarry@whoi.edu.
596
597 **Figure 1** – Map of the northwest coast of Costa Rica. Northern sites (blue) and central
598 sites (orange) as well as the plate boundary between the East Pacific Rise (EPR) crust
599 and Cocos Nazca spreading center (CNS) crust, and the Quesada Sharp Contortion (QSC)
600 are shown. Sample distances to trench (Supplementary Table 1) were calculated as the
601 distance of a line segment extending from the sample location, along the angle of

convergence, to the plate boundary[48]. Red-tipped triangles are volcanoes Orosí, Rincón dela Vieja, Miravalles, Tenorio, Arenal, Platanar, Poás, Barva, Turrialba, and Irazú, from north to south. Thin lines are depth to slab in 20km intervals[49]. Background data from GeoMapApp (http://www.geomapapp.org)[50].

Figure 2A – Helium isotopes ($^3He/^4He$) vs. distance from trench. The plot shows a decrease in $^3He/^4He$ trenchward, suggesting that there is pervasive deep slab/mantle degassing occurring across the entire arc, even though free CO_2 gas is absent. **2B** – carbon concentrations (as indicated by circle size) and $\delta^{13}C$ of CO_2 gas, dissolved inorganic carbon (DIC), dissolved organic carbon (DOC), and total organic carbon in sediments surrounding the surface emanation of the springs (sTOC) are shown vs. distance from trench and subduction zone section (**C**) in order to show the full range in data. These "bubble plots" show that there is a corresponding decrease in carbon concentrations and $\delta^{13}C$ values of DIC and DOC trenchward, and no change in concentrations and $\delta^{13}C$ values of TOC.

Figure 3 – Carbon isotopes as a function of DIC concentrations for northern (blue) and central (orange) DIC (filled symbols), along with isotope fractionation model in solid lines. DOC $\delta^{13}C$ values (open markers) as well as DOC concentrations (inset) correlate with those of DIC. For clarity, Santa Lucia (5.69 mmol/L DOC) is not included in inset. Values for arc gases (T ≥ boiling; plotted at 0% C sequestered as calcite) represent an endpoint of CO_2 concentration and $\delta^{13}C$, offset from DIC by the fractionation from gas to aqueous phase.

Figure 4A– Box model showing the carbon inputs[8] in the Costa Rica Forearc. Estimated inputs are from sediments, altered oceanic crust and serpentinized mantle via subduction. Estimated outputs are show for the forearc (this study) and the arc[2,8], as well as predicted transport to the deep mantle (inputs minus outputs). **4B** – Inset box model showing endmember carbon isotopic values into the forearc following

release from the slab/mantle. The model shows fluid pathways and associated fractionation as calcite forms, with approximately 91% of total carbon released in the forearc sequestered as calcite. The remaining dissolved carbon (DC) is isotopically depleted and partitioned into dissolved inorganic carbon (DIC) and dissolved organic carbon (DOC).

Methods:

Sample collection and analysis:

In 2017, fluid and gas samples were collected across two transects of the Costa Rican Arc (Figure 1), with pH ranging from 0.9-10.0 and temperatures ranging from 23-89°C. Fluid and gas samples were collected in evacuated glass flasks and Cu-tubes using standard collection procedures[51], whereby precautions were taken to minimize any possible air contamination[27]. Gas and fluids samples (n=24) from 2017 are accompanied by addition (n=17) samples collected during reconnaissance field campaigns in 2008, 2010 and 2012. He and C isotope data from the initial reconnaissance field campaigns were produced in the Fluids and Volatiles Laboratory at Scripps Institution of Oceanography (SIO), whereas data from 2017 are from Oxford (He-isotopes) and Tokyo Institute for Technology (C-isotopes).

Samples were collected over several field campaigns; however, all samples were collected during the dry season in an effort to minimize seasonal effects (Supplementary Table 1). Considering this, the data from the various labs are in good agreement. For example, fluids were collected at the Sabana Grande site in 2008, 2010 and again in 2017; C-isotope values of -12.69‰ (2017; Japan) agree well with -12.75‰ (2008; SIO), -12.79‰ (2008; SIO) and -13.43‰ (2012; SIO). He-isotope values for this site were 2.66 ± 0.13 R_A (2017; Oxford), 0.60 ± 0.03 R_A (2008; SIO) and 1.04± 0.11 R_A (2012: SIO), all indicate an admixture of radiogenic and mantle derived gases. Notably, there is not thought to be a discernable cosmogenic component in subduction-related fluids, as ^{3}He outputs greatly exceed input parameters[6]. Also,

much too little interplanetary dust particles is available to sustain the flux required. See Trull 1994. Also, high diffusivity of He in most low-T minerals is important. When considering the reproducibility of He isotope measurements, it is essential to consider the amount of air contamination in a given sample, which is estimated using the relative amount of He and Ne, expressed as the X-value ($^{4}He/^{20}Ne$ normalized to air). At Sabana Grande, the most pristine sample (highest X-value) yielded the highest He isotope value of 2.66 R_A (Extended Data Figure 2). Helium isotopes were also measured in samples collected at the Pueblo Antiguo site in 2010 (SIO), 2012 (SIO) and 2017 (Oxford), and in the two samples with high X-values (>5), the He isotopes measured at different laboratories are within analytical error (Oxford, 2017 = 4.34 ± 0.22 R_A and SIO, 2010 = 4.51 ± 0.11 R_A).

Gas and water samples from the 2008, 2010 and 2012 campaigns were analyzed at SIO for helium and carbon isotopes using instrumentation and protocols described previously[2,7,52]. All samples were extracted on a dedicated preparation line with a fraction of the non-condensable gas (containing He and Ne) captured in a 1720-glass breakseal. All CO_2 was condensed into a Pyrex breakseal following separation from water vapor, non-inert gases (N_2, CO, CH_4) and heavy noble gases (Ar, Kr and Xe).

Helium and neon analyses were carried out on a MAP-215 noble gas mass spectrometer SIO. First, the gas was released from the breakseal and prepared for analysis using a series of traps, held at liquid nitrogen temperature, and active-gas getters. Helium was separated from neon using a helium-cooled refrigeration stage interfaced to a trap lined with activated charcoal. All sample $^{3}He/^{4}He$ ratios were normalized to standard aliquots of air processed and analyzed under identical conditions.

Carbon dioxide was purified at SIO on a dedicated line using a variable temperature trap designed to separate CO_2 from sulfur-bearing species. Following

689 cleanup, the amount of CO_2 was measured using a capacitance gauge manometer in a
690 calibrated volume, prior to freezing an aliquot of the CO_2 in a Pyrex breakseal. For
691 isotope analysis, the CO_2 aliquot was inlet into a Thermo-Finnigan Delta XP^{Plus} Isotope
692 Ratio Mass Spectrometer (IRMS). Carbon isotopes on gas samples from the 2017
693 campaign were analyzed at Universidad Nacional on a Picarro G2201-I by acidification of
694 NaOH solutions extracted from Giggenbach bottle samples. $\delta^{13}C_{PDB}$ values were
695 calibrated against a set of 8 standards with values ranging from + 2.42 ‰ to -37.21‰,
696 including internationally accepted standards NBS19 and Carrara Marble. Reported delta
697 values have uncertainties of <0.1 ‰ based on repeat analyses of standards and samples.
698
699 Noble gas analysis was also conducted in the Noble Laboratory at the University
700 of Oxford (2017 samples), using a dual mass spectrometer setup, interfaced to a
701 dedicated extraction and purification system[53]. Gases were collected in Cu-tubes, and
702 then transferred to the extraction and purification line where reactive gases were
703 removed by exposing gases to a titanium sponge held at 950 °C. The titanium sponge
704 was cooled for 15 minutes to room temperature before gases were expanded to a dual
705 hot (SAES GP-50) and cold (SAES NP-10) getter system, held at 250 °C and room
706 temperature, respectively. A small aliquot of gases was segregated for preliminary
707 analysis on a Hiden Analytical HAL-200 quadrupole mass spectrometer. All noble gases
708 were then concentrated using a series of cryogenic traps; heavy noble gases (Ar-Kr-Xe)
709 were frozen down at 15 K on an all SS finger and the He and Ne were frozen down at 19
710 K on a cold finger filled with charcoal. The temperature on the charcoal finger was then
711 raised to 34 K to release only He, which was inlet into a Helix SFT mass spectrometer.
712 Following He analysis, the temperature on the charcoal cryogenic trap was raised to 90
713 K to release Ne, which was inlet into an ARGUS VI mass spectrometer.
714
715 Water samples for carbon isotope analysis (2017 samples) of dissolved inorganic
716 carbon (DIC), dissolved organic carbon (DOC) were collected by 50-mL syringes and
717 filtered by connecting membrane syringe filters with a pore size of 0.20 µm (DISMIC–

718 25AS; Advantec Toyo Kaisha, Tokyo, Japan) and syringe needle. Then filtered water was
719 directly injected to the pre-vacuumed 50-mL serum bottle sealed with butyl rubber
720 septa and an aluminum crimp. The subsampled water (10 mL) for DIC measurement
721 from each water sample of 50-mL sealed vials by nitrogen gas and transferred to a pre-
722 vacuumed 30-mL glass vial sealed with butyl rubber septa and an aluminum crimp. DIC
723 concentrations and their $\delta^{13}C$ values were measured using CO_2 in the headspace of glass
724 vials after a 1-h reaction with injected 0.5mL H_3PO_4. DOC were also measured CO_2 in the
725 headspace after the reaction of carbonate-free residue with 0.2 g sodium persulfate.
726 The amount of CO_2 and the isotopic values were measured using a Agilent 6890N gas
727 chromatograph attached to a Thermo-Finnigan Delta XP^{Plus}. Two international standards
728 ($\delta^{13}C$ = −13.90‰ and 2.52‰) were used for standardization, and the standard
729 deviations were shown by over 3 times measurement.
730
731 The sediments surrounding the surface emanations of the springs were collected
732 for measuring TOC content and carbon isotopic compositions. The sediment samples
733 were kept at 4°C until transporting to the laboratory. Glass vial samples were then
734 stored at −80°C until further treatment. Firstly, the sediment samples were freeze-dried
735 and then crushed into fine grains using a mortar to remove large leaves and roots. 50–
736 100 mg of sediment samples were weighed and reacted with 1 M HCl solution until
737 effervescence stopped, followed by a rinse with distilled water until the pH neutralized.
738 The TOC sediment samples were analyzed using an elemental analyzer (EA-1110;
739 Thermo Fisher Scientific) coupled to a Thermo Fisher Scientific MAT 252 isotope ratio
740 mass spectrometer (IRMS).
741
742 Samples for cell counts were taken in 2017 as close to the source spring as
743 possible, usually in an outflow from a rock outcrop or a small surface pool that was
744 rapidly being refilled by the source. We placed 1 ml fluids into a 2 ml plastic tube with a
745 rubber o-ring screwcap (to prevent evaporation) containing 500 µl 3%
746 paraformaldehyde solution in phosphate-buffered-saline (PBS). Cell count samples fixed

747 with 3% paraformaldehyde in the field were kept at room temperature during return to
748 the University of Tennessee and were weighed upon returning to the lab. Cell counts
749 were determined on a Guava Easy Cyte 6HT-2L (Millipore) flow cytometer. Triplicate
750 aliquots of each sample (200µL) were stained with 5× SybrGreen prior to analysis. We
751 estimated contributions of cell biomass with total cell counts, and average carbon
752 content of subsurface microbes[54], by multiplying the average number of cells in our fluid
753 samples by the volume of hosting rocks (from the trench to the arc – assuming a log
754 increase of the isotherms moving toward the arc) up to 2 km depths, and using an
755 average rock porosity (to obtain possible fluid amounts)[55], and found that they did
756 represent a significantly large carbon reservoir.
757
758 Aliphatic hydrocarbons (C10-C40) and polycyclic aromatic hydrocarbons
759 (PAHs) were analyzed using conventional procedures based on gas chromatography
760 with a flame ionization detector (FID) and HPLC with diode array and fluorimetric
761 detection[56]. Briefly, aliphatic hydrocarbons (C10-C40) were extracted with
762 hexane:acetone (2:1) in a microwave (110°C for 25 min, 800 Watt) (Mars CEM, CEM
763 Corporation, Matthews NC). After centrifugation at 3.000 × g for 10 min, the
764 supernatants were purified with solid-phase extraction (Phenomenex Strata-X, 500
765 mg × 6 mL plus Phenomenex Strata-FL, 1000 mg × 6 mL) and then concentrated using
766 a SpeedVac (RC1009; grade n-hexane and analyzed with a PerkinElmer gas
767 chromatograph) equipped with an Elite-5 capillary column (30 mm × 0.32 mm ID ×
768 0.25 µm-df) and a FID. For quantitative determination, the system was calibrated
769 with an unsaturated pair n-alkane standard mixture according to ENISO 9377-3 (Fluka
770 68281). For the analysis of PAHs, sediment samples were extracted using 0.5 M
771 potassium hydroxide in methanol with microwave at 55°C for 20 min (800 Watt)
772 (CEM, Mars System). After centrifugation at 3.000 × g for 10 min, the methanol
773 extracts were concentrated using a SpeedVac and purified with solid-phase
774 extraction (Octadecyl C18, 500 mg × 6 mL, Bakerbond). A final volume of 1 mL was
775 recovered with pure, analytical HPLC gradient grade acetonitrile; HPLC analyses were

carried out in a water-acetonitrile gradient by fluorimetric and diode array detection. The PAHs were identified according to the retention times of an appropriate pure standards solution (EPA 610 Polynuclear Aromatic Hydrocarbons Mix), and classified as low molecular weight (LMW: naphthalene, acenaphthylene, 1-methyl naphthalene, 2-methyl naphthalene, acenaphthene, fluorene, phenanthrene, anthracene) or high molecular weight (HMW: fluoranthene, pyrene, benzo(a)antrhacene, chrysene, 7,12-dimethyl-benzo(a)anthracene, benzo(b)fluoranthene, benzo(k)fluoranthene, benzo(a)pyrene, dibenzo(a,h)anthracene, benzo(g,h,i)perylene, indeno(1,2,3-cd)pyrene). Accuracy and precision were checked analyzing both pure standard solutions and reference materials (NIST 1944) and the obtained concentrations were always within the 95% confidence intervals of certified values. Aliquots of all the samples were dried in a oven at 60°C for at least 8 h, up to obtain a constant weight, in order to quantify the interstitial water content, allowing to express all the analyzed chemicals as a function of the dry weight (d.w.) of the sediments.

Isotope fractionation modeling:

He-C studies in volcanic arc settings[2,57-60] have coupled helium and carbon isotopes to distinguish carbon from different provenances using a three-component mixing model (Extended Data Figure 1). In such acidic settings, volcanic activity has been suggested to release previously sequestered CO_2[61-64], which mixes with slab/mantle carbon and results in the characteristic signatures. Samples from this study were collected from a range of lithologies from ophiolites in Nicoya[65-70] to andesitic and basaltic volcanic rocks in the arc and forearc. The volcanic front in Costa Rica developed on the western edge of the Caribbean Plateau, an oceanic plate basement without any preexisting continental or arc material[71-73]. The Santa Elena ophiolite is part of a series of exotic, arc-related terrenes that make the basement of the volcanic front in southern Nicaragua and does not extend south of the Hess Escarpment-Santa Elena suture[74-75]. However, these carbon isotope data are consistent with a model that requires for a

homogenous C isotope input flux. This indicates that degassing of the downgoing slab/mantle drives the ^{13}C-isotope inputs, rather than the over-riding crust, but in some cases, this signal is subsequently obfuscated by low temperature precipitation of isotopically heavy calcite, which effectively fractionates the carbon isotopes. Here we provide additional details on the fractionation modeling used to construct the calcite fractionation curves in Figure 3 (main text).

In summary, CO_2 is released from the slab/mantle and reacts with shallow groundwater forming an initial DIC pool (dissolved CO_2). A fractionation factor (see details below) is calculated based on temperature (assumed to be 67°C in the northern transect and 63°C in the central transect) and an alpha value for CO_2-HCO_3^--$CaCO_3$, where $CaCO_3$ is calcite. The starting $\delta^{13}C$ input is determined to be different from the northern (5.0‰) and central (0.5‰) transect, presumably controlled by different slab inputs. Notably, the presumed slab inputs are consistent with positive isotope values measured in carbonate sediments off the coast of Nicoya[76]. Starting $\delta^{13}C$ input conditions are assumed to be the same for forearc, backarc and arc. DOC is in isotopic equilibrium with DIC at these temperatures and assumed alpha values. The DIC is transformed from CO_2 to HCO_3^- in alkaline waters and the resulting DIC concentrations are not affected by further dilution of meteoric water or by concentration due to steam loss. As the Rayleigh fractionation progresses, the DIC in the forearc is consumed and a Rayleigh fractionation occurs. Open system fractionation (Rayleigh distillation) curves were iteratively fitted to the data using:

eq. 1.

$$\delta^{13}C_{DC_f} \cong \left(\delta^{13}C_{DC_i} + 1000\right)\left(F^{\alpha_{DC-calcite}-1}\right) - 1000$$

after[77], where F is the fraction of dissolved carbon (DC) remaining in the fluid, $\delta^{13}C_{DC_f}$ is the carbon isotope composition of DC at F, $\delta^{13}C_{DC_i}$ is the initial isotope composition of the DC, and $\alpha_{DC\text{-}calcite}$ is the fractionation factor between DC and calcite at a given temperature. The fractionation factor between DC and calcite was calculated from[78]:

eq. 2.

$$1000ln\alpha_{DC-calcite} = -8.91x10^{8}T^{-3} + 8.557x10^{6}T^{-2} - 1.881x10^{4}T^{-1} + 8.27$$

where T is the temperature in Kelvin.

Model curves were fit to the data from each transect by iteratively varying the values of $\delta^{13}C_{DC_i}$ and the temperature of calcite formation. Best fit results were obtained with $\delta^{13}C_{DC_i} = +5.0‰$ and T = 67 °C (R^2 = 0.91) for the northern transect and $\delta^{13}C_{DC_i} = +0.5‰$ and T = 63 °C (R^2 = 0.86) for the central transect.

Total dissolved carbon (DC) values used in the model are calculated from the sum of measured DIC and DOC concentrations (Supplementary Table 4), and $\delta^{13}C_{DC}$ is the average of $\delta^{13}C_{DIC}$ and $\delta^{13}C_{DOC}$, weighted by their respective DIC and DOC concentrations. DIC dominates total DC contents, typically accounting for ~80% of DC on a sample by sample basis. DOC data are not available for 12 of our 30 samples, as several samples were collected on previous reconnaissance field campaigns. However, the strong correlation between DC and DIC (Extended Data Figure 3) allows us to confidently predict the DC concentration and $\delta^{13}C_{DC}$ of the samples for which DOC is not available. The predicted DC and $\delta^{13}C_{DC}$ are thus used for the 12 samples for which DOC data are not available in Figure 3 (main text). The slope of the linear regressions in Figures S2a and S2c is used to calculate the fraction of DOC in the northern and central transects (5.4 % and 4.7 %, respectively).

Carbon budget calculations:

The carbon isotope fractionation model allows calculation of the fraction of carbon in various forearc reservoirs. Based on the average $\delta^{13}C_{DC}$ values at the forearc sites (here defined as located at <155 km from the trench), the fraction (F) of carbon

remaining in the fluid can be calculated (expressed as "% carbon sequestered as calcite" in Figure 3, which is equal to 100(1- F)). The average $\delta^{13}C_{DC}$ values at forearc sites are further used to calculate the total DC concentration in mmol/L based on the Rayleigh curves. Because the curves are steep at low F values, the $\delta^{13}C_{DC}$ values represent a more robust and sensitive parameter than DC concentrations, which are more susceptible to dilution and analytical uncertainty at low concentrations. The average DIC concentration for forearc fluid is then calculated from dissolved carbon concentrations from the relationship between DC and DIC expressed in Figures S2a and S2c. In this model, DOC is then the residual carbon once DIC and calcite concentrations are accounted for. The results of these calculations indicate that 91.3% of the total forearc carbon is sequestered as calcite, 6.0% is released at the surface as DIC, and 2.7% is consumed by microbiological processes to form DOC.

Our flux estimates for the Costa Rican forearc (see main text) show that between 7.1 x 10^6 and 7.9 x 10^8 mol CO_2/yr are released to the surface by spring outflow as DIC and CO_2 gas. Based on the above-described model, we argue that this represents the residual carbon left over after pervasive calcite deposition. The total flux (i.e., subducted slab and mantle fluid) through the forearc, including both calcite deposition and microbial consumption, ranges from 1.2 x 10^8 to 1.3 x 10^{10}mol/yr (Figure 4).

Previous Mass Balance calculations:

To put our forearc flux estimate into context, we must consider previous flux estimates, which to date, have focused mostly on high temperature regions[11-13], where there is a distinct point-source for carbon emissions. However, little work has been conducted in the forearc of Costa Rica[3] even though thermodynamic modeling of the Costa Rica convergent margin predicts efficient CO_2 release from the top of the subducting slab beneath forearcs, at depths of 65-80 km[12].

Past budget approaches[58] coupled He and C isotopes to tease apart C sourced from different provenances using a three-component mixing model (Fig. S1). Subducted slab carbon is presumed to derive from carbonate rocks and have a value of ~0 VPDB, mantle values are assumed to be approximately –6.5 ± 2.0‰ and isotopically low carbon isotope values are attributed to contributions from organic sediments (-30‰). Here we argue that in the forearc environment these values do not result from mixing, but instead from low temperature calcite precipitation and biological consumption.

Arc fluxes are typically only measured along a relatively narrow transect source: the volcanic front. In contrast, springs occur over a large stretch of the forearc, so this is a much larger area to integrate. Quantitative assessment of gas fluxes from the forearc, backarc, fault-related sites, hydrothermal volcanic systems (e.g., Tenorio, Miravalles, Irazú, Rincón de la Vieja flank sites), and concurrent diffuse degassing are lacking. Here we place better constraints on forearc fluxes, which complement recent constraints on magmatic C fluxes[8]. We estimate a flux between of 1.2×10^8 and 1.3×10^{10} to mol CO_2 per year, which represents as much as ~36% of the total arc flux. , and could reduce the amount transferred into the deep mantle by up to ~19%.

Previous studies have utilized helium and carbon isotopes ($^3He/^4He$, $\delta^{13}C$) and relative abundances ratios ($CO_2/^3He$) of fumarole sites at arc settings. Two approaches were taken in these areas in order to determine CO_2 fluxes: 1) combining measured $CO_2/^3He$ data with known ^3He fluxes and 2) to combine measured CO_2/SO_2 data with known SO_2 fluxes. Previous work was conducted throughout Costa Rica[3,6,8] El Salvador Honduras[7] and Nicaragua[2].

In typical subduction zones, the vast majority of carbon is thought to be recycled back into the lithosphere, hydrosphere, and atmosphere[1], and what remains is transported into the deep mantle. In stark contrast, mass balance considerations from the Costa Rica convergent margin suggest the majority of subducted C (more than 85%)

920 is ultimately transferred into the deep mantle[2,3,6]. Importantly, this estimation assumes
921 that the forearc and backarc fluxes are negligible, which we have shown in this
922 contribution to be untrue. Prior work[6] estimated the subducting CO_2 input flux for ~310
923 km Arc of Costa Rica to be 8.2×10^{10} mol/yr[6], assuming "1% organic CO_2" in sediments
924 based on data from a single IODP site (1039) and a "global average" altered crustal
925 composition of 0.2% CO_2, extrapolated over the entire slab thickness. Published carbon
926 degassing (output) flux estimates vary between 1.2×10^{10} mol/yr to 1.5×10^{10} mol/yr,
927 with an average value of 1.26×10^{10} mol/yr. Importantly, these estimates are
928 determined to be >90% sediment and marine carbonate derived, based on C-isotope
929 data[2]. However, more recent studies[8,61,79] use a more complete assessment of volcanic
930 degassing from the arc to show that the current volcanic CO_2 flux from Costa Rica is
931 significantly higher (6.10×10^{10} mol/yr). The 2017 study[8] is based on new data for 11
932 volcanoes in Costa Rica and Nicaragua showing that the CO_2 flux from the arc is
933 underestimated in previous studies. Their finding suggests that the Central American
934 subduction margin may be more similar to other arc segments[1] than previously
935 thought[2,6]. The 2017 findings[8] suggest the 2014-2015 CO_2 flux from the Costa Rican arc
936 is an order of magnitude greater than previous estimates[2,6]. However, the Costa Rican-
937 Nicaraguan margin has displayed an increase in arc-wide volcanic activity in recent
938 years[8]. Thus, arc systems probably show significant variation in gas output over time. If
939 the older estimates[2,6] of CO_2 flux are taken to be more representative of the time-
940 integrated CO_2 flux, then there is still a considerable missing flux in the forearc or arc. In
941 Figure 4 we take the average value from references 2 and 8 to determine an average
942 CO_2 flux of 3.7 mol/yr ± 66%.
943
944 **Geologic Background:**
945 The Central American subduction zone is characterized by rapid (70–90 mm/year)
946 convergence of young (15–25 Ma) oceanic lithosphere[80-82], whereas the downgoing Cocos
947 plate is composed of a thin sedimentary layer (~428m). The upper section of the column
948 (177 m) consists of Quaternary to upper Miocene hemipelagic diatomaceous mud and

middle Miocene brown abyssal clay and the lower section consists of middle–lower Miocene chalky carbonate ooze and manganiferous chalk and chert[83-84]. The composition of subducted sediments and carboniferous material is microbiologically altered, due to the fact that anaerobic respiration and fermentation determine sediment redox conditions, alkalinity, and carbon isotope pools[85-86]. The entire column of incoming sediments under-thrusts the toe of the Caribbean Plate. However, the absence of significant off-scraping or sediment accretion suggests the Costa Rica convergent margin is either non-accretionary, or underplated further landward[79,87]. Under-thrusting leads to rapid compaction of the upper hemipelagic sediments and dewatering of pore fluids within the first few kilometers of subduction[88], resulting in the release of carbon dioxide and methane at relatively shallow depths into the overlying forearc[3]. Fluids released during dehydration reactions ascend through the overriding plate along deep-penetrating faults, producing numerous fluid venting sites in the forearc of Costa Rica[89]. A significant portion of the forearc is subaerial (Nicoya and Osa peninsulas), providing unique sampling opportunities not found at the majority of arc systems. In addition to mechanically induced shallow dewatering near the toe of the overriding plate, deeply-sourced (i.e., abiotic) fluids are released by mineral dehydration reactions and phase transformations at depths of approximately 10-15 km (between 60-140°C)[88,90], which are pressure and temperature ranges that are within the range of theoretically habitable environments for microorganisms[91-92]. Volcanoes in Costa Rica form a part of the southern segment of the Central American Volcanic Arc. The volcanic arc in Costa Rica extends from the north to the center of Costa Rica, immediately to the east of the Nicoya Peninsula. We collected samples for this study in the forearc, arc and backarc of this region.

Microbiological Background:

^{13}C-depleted carbon dioxide in fluids released in the submarine portion of the outer forearc indicate a δ^{13}C depleted source and may imply biological production through anaerobic respiration of sulfate, which is an abundant oxidant in seawater (Füri et al. 2010). The level of ^{13}C-depletion can be moderate (-10 to -15‰),

suggesting electron donors from organic matter, or extreme (-60 to -70‰), suggesting electron donors from methane. Methanotrophy can occur anaerobically through sulfate reduction[93], or aerobically when oxygenated seawater mixes with methane-rich fluids[94]. The methane itself may be methanogenic products mobilized from the >12 km source fluids[95], or shallower methanogenesis[96], but this has yet to be resolved with isotopic analysis.

Methane in the subaerial section of the margin has been found to have a significant biogenic component, with $\delta^{13}C$ of -35 to -45‰, and presence of methanogenic archaea[97-98]. However, no large-scale survey of the effects of microbiology on degassing across a convergent margin have been performed. The few microbiological studies that have been performed in convergent margins have focused on a single site at a time, preventing any region-scale exploration of how microbes interact with these deep geological processes.

Methods References:

51. Giggenbach, W.F., Goguel, R.L. Methods for the collection and analysis of geothermal and volcanic water and gas samples, Rep. CD 2387, Chem. Div., Dept. of Sci. and Ind. Res., Petone, N. Z, , p. 53. (1989).

52. Kulongoski, J. T., & Hilton, D. R. A quadrupole-based mass spectrometric system for the determination of noble gas abundances in fluids. *Geochemistry, Geophysics, Geosystems*, 3(6), 1-10. (2002).

53. Barry, P. H., Lawson, M., Meurer, W. P., Warr, O., Mabry, J. C., Byrne, D. J., & Ballentine, C. J. Noble gases solubility models of hydrocarbon charge mechanism in the Sleipner Vest gas field. *Geochimica et Cosmochimica Acta*, 194, 291-309. (2016).

54. Braun, S., Morono, Y., Becker, K.W., Hinrichs, K.U., Kjeldsen, K.U., Jørgensen, B.B. and Lomstein, B.A. Cellular content of biomolecules in sub-seafloor microbial communities. *Geochimica et Cosmochimica Acta*, 188, pp.330-351. (2016).

55. Giovannelli, D., d'Errico, G., Fiorentino, F., Fattorini, D., Regoli, F., Angeletti, L., et al. Diversity and Distribution of Prokaryotes within a Shallow-Water Pockmark Field. *Front. Microbiol.* 7. (2016).

56. McMahon, S., & Parnell, J. Weighing the deep continental biosphere. FEMS Microbiology Ecology, 87(1), 113-120. (2014).

57. Sano, Y., & Marty, B. Origin of carbon in fumarolic gas from island arcs. *Chemical Geology*, 119(1-4), 265-274. (1995).

58. Snyder, G., Poreda, R., Hunt, A., & Fehn, U. Regional variations in volatile composition: Isotopic evidence for carbonate recycling in the Central American volcanic arc. *Geochemistry, Geophysics, Geosystems*, *2*(10). (2001).

59. Snyder, G., Poreda, R., Fehn, U., & Hunt, A. The geothermal fields of Central America: influence of the subduction process on its volatile composition. *Geological Magazine of Central America* , (30). (2004).

60. Wehrmann, H., Hoernle, K., Portnyagin, M., Wiedenbeck, M., & Heydolph, K. Volcanic CO2 output at the Central American subduction zone inferred from melt inclusions in olivine crystals from mafic tephras. *Geochemistry, Geophysics, Geosystems*, *12*(6). (2011).

61. de Moor, J. M., Aiuppa, A., Avard, G., Wehrmann, H., Dunbar, N., Muller, C., Tamburello, G., Giudice, G., Liuzzo, M., Moretti, R. & Conde, V. Turmoil at Turrialba Volcano (Costa Rica): Degassing and eruptive processes inferred from high-frequency gas monitoring. *Journal of Geophysical Research: Solid Earth*, *121*(8), 5761-5775. (2016).

62. Dawson, P., Chouet, B., & Pitt, A. Tomographic image of a seismically active volcano: Mammoth Mountain, California. *Journal of Geophysical Research: Solid Earth*, *121*(1), 114-133. (2016).

63. Mason, E., Edmonds, M., & Turchyn, A. V. Remobilization of crustal carbon may dominate volcanic arc emissions. *Science*, *357*(6348), 290-294. (2017).

64. Chiodini, G., Pappalardo, L., Aiuppa, A., & Caliro, S. The geological CO2 degassing history of a long-lived caldera. *Geology*, *43*(9), 767-770. (2015).

65. Berrange, J. P., & Thorpe, R. S. The geology, geochemistry and emplacement of the Cretaceous—Tertiary ophiolitic Nicoya Complex of the Osa Peninsula, southern Costa Rica. *Tectonophysics*, *147*(3-4), 193-220. (1988).

66. Giggenbach, W. F. Relative importance of thermodynamic and kinetic processes in governing the chemical and isotopic composition of carbon gases in high-heatflow sedimentary basins. *Geochimica et Cosmochimica Acta*, *61*(17), 3763-3785. (1997).

67. Kuijpers, E. P. The geologic history of the Nicoya Ophiolite Complex, Costa Rica, and its geotectonic significance. *Tectonophysics*, *68*(3-4), 233-255. (1980).

68. Schwarzenbach, E. M., Lang, S. Q., Früh-Green, G. L., Lilley, M. D., Bernasconi, S. M., & Méhay, S. Sources and cycling of carbon in continental, serpentinite-hosted alkaline springs in the Voltri Massif, Italy. *Lithos*, *177*, 226-244. (2013).

69. Torgersen, T. Terrestrial helium degassing fluxes and the atmospheric helium budget: Implications with respect to the degassing processes of continental crust. *Chemical Geology: Isotope Geoscience Section*, *79*(1), 1-14. (1989).

70. Walther, C. H. E., Flueh, E. R., Ranero, C. R., Von Huene, R., & Strauch, W. Crustal structure across the Pacific margin of Nicaragua: Evidence for ophiolitic basement and a shallow mantle sliver. *Geophysical Journal International*, *141*(3), 759-777. (2000).

71. Gazel, E., Denyer, P., & Baumgartner, P. O. Magmatic and geotectonic significance of santa elena peninsula, costa rica. *Geologica Acta*, *4*(1-2), 0193-202. (2006).

72. Gazel, E., Hoernle, K., Carr, M. J., Herzberg, C., Saginor, I., Van den Bogaard, P., Hauff, F., Feigenson, M., & Swisher, C. Plume–subduction interaction in southern Central America: Mantle upwelling and slab melting. *Lithos*, *121*(1), 117-134. (2011).

73. Gazel, E., Hayes, J. L., Hoernle, K., Kelemen, P., Everson, E., Holbrook, W.S., Hauff, F., Van Den Bogaard, P., Vance, E.A., Chu, S., & Calvert, A. J.

Continental crust generated in oceanic arcs. *Nature Geoscience*, *8*(4), 321. (2015).

74. Madrigal, P., Gazel, E., Denyer, P., Smith, I., Jicha, B., Flores, K.E., Coleman, D. & Snow, J. A melt-focusing zone in the lithospheric mantle preserved in the Santa Elena Ophiolite, Costa Rica. *Lithos*, *230*, 189-205. (2015).

75. Madrigal, P., Gazel, E., Flores, K. E., Bizimis, M., & Jicha, B. Record of massive upwellings from the Pacific large low shear velocity province: Nature Communications, v. 7, p. 13309. (2016).

76. Li, L., & Bebout, G. E. Carbon and nitrogen geochemistry of sediments in the Central American convergent margin: Insights regarding subduction input fluxes, diagenesis, and paleoproductivity. *Journal of Geophysical Research: Solid Earth*, 110(B11). (2005).

77. Holloway, J. R., & Blank, J. G. Application of experimental results to COH species in natural melts. *Reviews in mineralogy*, 30, 187-187. (1994).

78. Ohmoto, H., & Rye, R. O. Isotopes of sulfur and carbon. *Geochemistry of Hydrothermal Ore Deposits (Barnes, HL, ed.)*, 509-567. (1979).

79. de Moor, J. M., Aiuppa, A., Pacheco, J., Avard, G., Kern, C., Liuzzo, M., Martinez, M., Giudice, G., & Fischer, T. P. Short-period volcanic gas precursors to phreatic eruptions: Insights from Poás Volcano, Costa Rica. *Earth and Planetary Science Letters*, *442*, 218-227. (2016).

80. Kimura, G., et al. (Eds.) Proceedings of the Ocean Drilling Program, *Initial Reports, vol. 170, Ocean Drill. Program*, College Station, Tex. (1997).

81. Barckhausen, U., Ranero, C. R., Huene, R. V., Cande, S. C., & Roeser, H. A. Revised tectonic boundaries in the Cocos Plate off Costa Rica: Implications for the segmentation of the convergent margin and for plate tectonic models. *Journal of Geophysical Research: Solid Earth*, 106(B9), 19207-19220. (2001).

82. DeMets, C. A new estimate for present day Cocos Caribbean plate motion: Implications for slip along the Central American volcanic arc. *Geophysical Research Letters*, 28(21), 4043-4046. (2001).

83. Patino, L. C., Carr, M. J., & Feigenson, M. D. Local and regional variations in Central American arc lavas controlled by variations in subducted sediment input. *Contributions to Mineralogy and Petrology*, 138(3), 265-283. (2000).

84. von Huene, R., Langseth, M., Nasu, N., & Okada, H. A summary of Cenozoic tectonic history along the IPOD Japan Trench transect. *Geological Society of America Bulletin*, 93(9), 829-846. (1982).

85. Parkes, R. J., Cragg, B. A., Fry, J. C., Herbert, R. A., & Wimpenny, J. W. T. Bacterial biomass and activity in deep sediment layers from the Peru margin. *Phil. Trans. R. Soc. Lond. A*, 331(1616), 139-153. (1990).

86. Biddle, J.F., Lipp, J.S., Lever, M.A., Lloyd, K.G., Sørensen, K.B., Anderson, R., Fredricks, H.F., Elvert, M., Kelly, T.J., Schrag, D.P. and Sogin, M.L. Heterotrophic Archaea dominate sedimentary subsurface ecosystems off Peru. *Proceedings of the National Academy of Sciences*, 103(10), 3846-3851. (2006).

87. Vannucchi, P., and Tobin, H. Deformation structures and implications for fluid flow at the Costa Rica convergent margin, ODP Sites 1040 and 1043, Leg 170, *Journal of Structural Geology*, 22(8), 1087–1103. (2000).

88. Spinelli, G. A., and Underwood, M. B. Character of sediments entering the Costa Rica subduction zone: Implications for partitioning of water along the plate interface, *Isl. Arc*, 13(3), 432–451. (2004).

89. Ranero, C.R., Grevemeyer, I., Sahling, H., Barckhausen, U., Hensen, C., Wallmann, K., Weinrebe, W., Vannucchi, P., Von Huene, R. and McIntosh, K. Hydrogeological system of erosional convergent margins and its influence on tectonics and interplate seismogenesis. *Geochemistry, Geophysics, Geosystems*, 9(3). (2008).

90. Spinelli, G. A., and Saffer, D. M. Along-strike variations in underthrust sediment dewatering on the Nicoya margin, Costa Rica related to the updip limit of seismicity, *Geophysical Research Letters*, 31, L04613. (2004).

91. Lloyd, K. G., Edgcomb, V. P., Molyneaux, S. J., Boer, S., Wirsen, C. O., Atkins, M. S., & Teske, A. Effects of dissolved sulfide, pH, and temperature on growth and survival of marine hyperthermophilic archaea. *Applied and Environmental Microbiology*, 71: 6383-6387. (2005).

92. Edgcomb, V.P., Molyneaux, S.J., Böer, S., Wirsen, C.O., Saito, M., Atkins, M.S., Lloyd, K. and Teske, A. Survival and growth of two heterotrophic hydrothermal vent archaea, Pyrococcus strain GB-D and Thermococcus fumicolans, under low pH and high sulfide concentrations in combination with high temperature and pressure regimes. *Extremophiles*, 11(2), 329-342. (2007).

93. Marlow, J. J., Steele, J. A., Ziebis, W., Thurber, A. R., Levin, L. A., & Orphan, V. J. Carbonate-hosted methanotrophy represents an unrecognized methane sink in the deep sea. *Nature Communications*, 5, 5094. (2014).

94. Boetius, A., & Wenzhöfer, F. Seafloor oxygen consumption fuelled by methane from cold seeps. *Nature Geoscience*, 6(9), 725. (2013).

95. Hensen, C., Wallmann, K., Schmidt, M., Ranero, C. R., & Suess, E. Fluid expulsion related to mud extrusion off Costa Rica—a window to the subducting slab. *Geology*, 32(3), 201-204. (2004).

96. Colwell, F. S., Boyd, S., Delwiche, M. E., Reed, D. W., Phelps, T. J., & Newby, D. T. Estimates of biogenic methane production rates in deep marine sediments at Hydrate Ridge, Cascadia Margin. *Applied and environmental microbiology*, 74(11), 3444-3452. (2008).

97. Sánchez-Murillo, R., Gazel, E., Schwarzenbach, E. M., Crespo-Medina, M., Schrenk, M. O., Boll, J., & Gill, B. C. Geochemical evidence for active tropical serpentinization in the Santa Elena Ophiolite, Costa Rica: An analog of a humid early Earth?. *Geochemistry, Geophysics, Geosystems*, 15(5), 1783-1800. (2014).

98. Crespo-Medina, M., Twing, K. I., Kubo, M. D., Hoehler, T. M., Cardace, D., McCollom, T., & Schrenk, M. O. Insights into environmental controls on microbial communities in a continental serpentinite aquifer using a microcosm-based approach. *Frontiers in microbiology*, 5, 604. (2014).

Data Availability Statement (DAS):

All raw data needed to make the plots are available in Tables 1 and 2 as well as in the Source Data file provided. All data is archived through EarthChem (DOI: 10.1594/IEDA/111271)

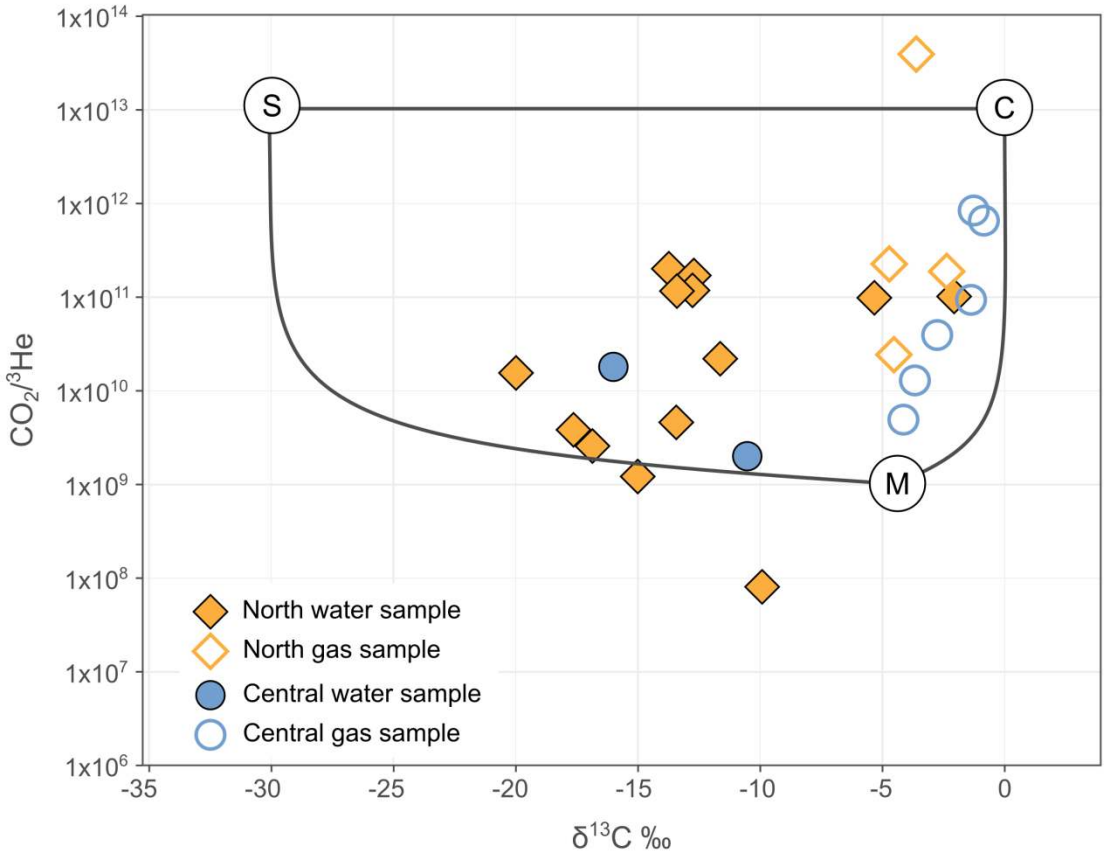

Extended Data Figure 1 – $CO_2/^3He$ vs. $\delta^{13}C$ for all samples collected, together with endmember mixing lines between mantle, organic sediment and carbonate endmembers. We argue that such mixing relationships cannot easily explain the water data, and instead carbon isotope fractionation associated with calcite precipitation and chemolithoautotrophy introduces the observed $\delta^{13}C$ variations.

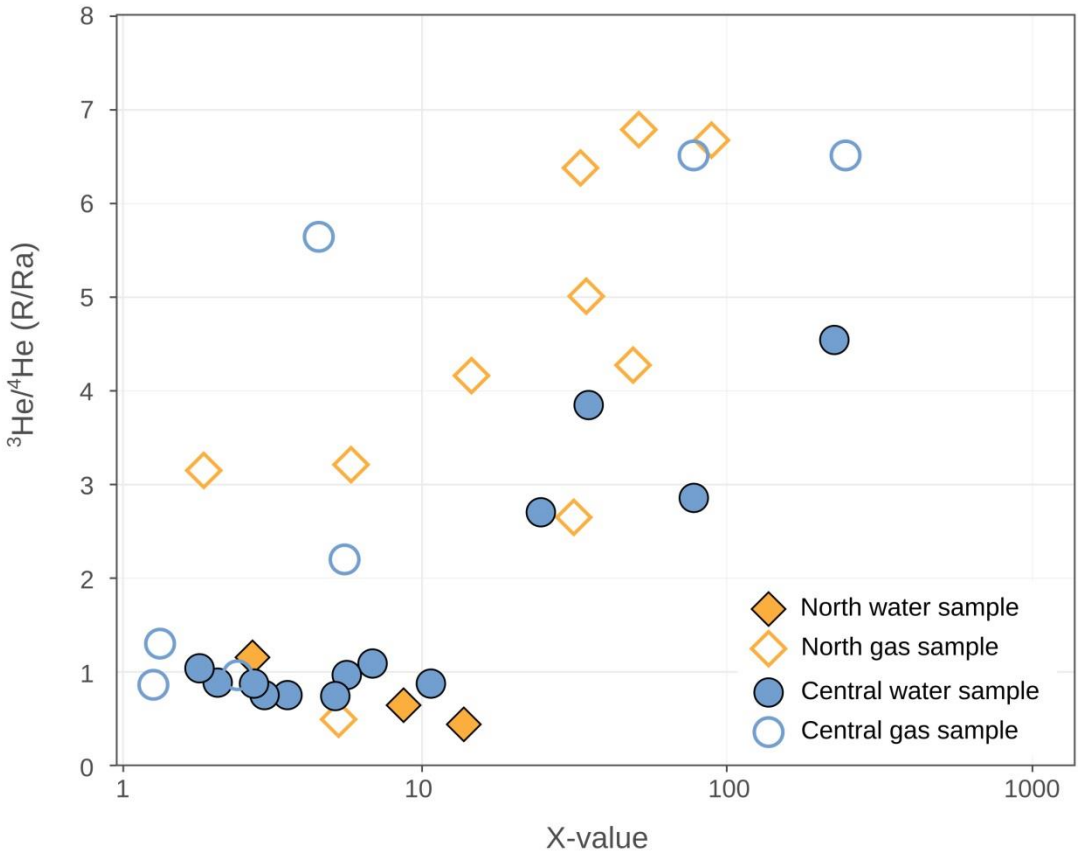

Extended Data Figure 2 – Helium isotopes ($^3He/^4He$) vs. X-values (air-normalized $^4He/^{20}Ne$; considering solubility in water for fluid samples[23]). The majority of samples have high (>5) X-values, indicating minimal air-contributions to samples.

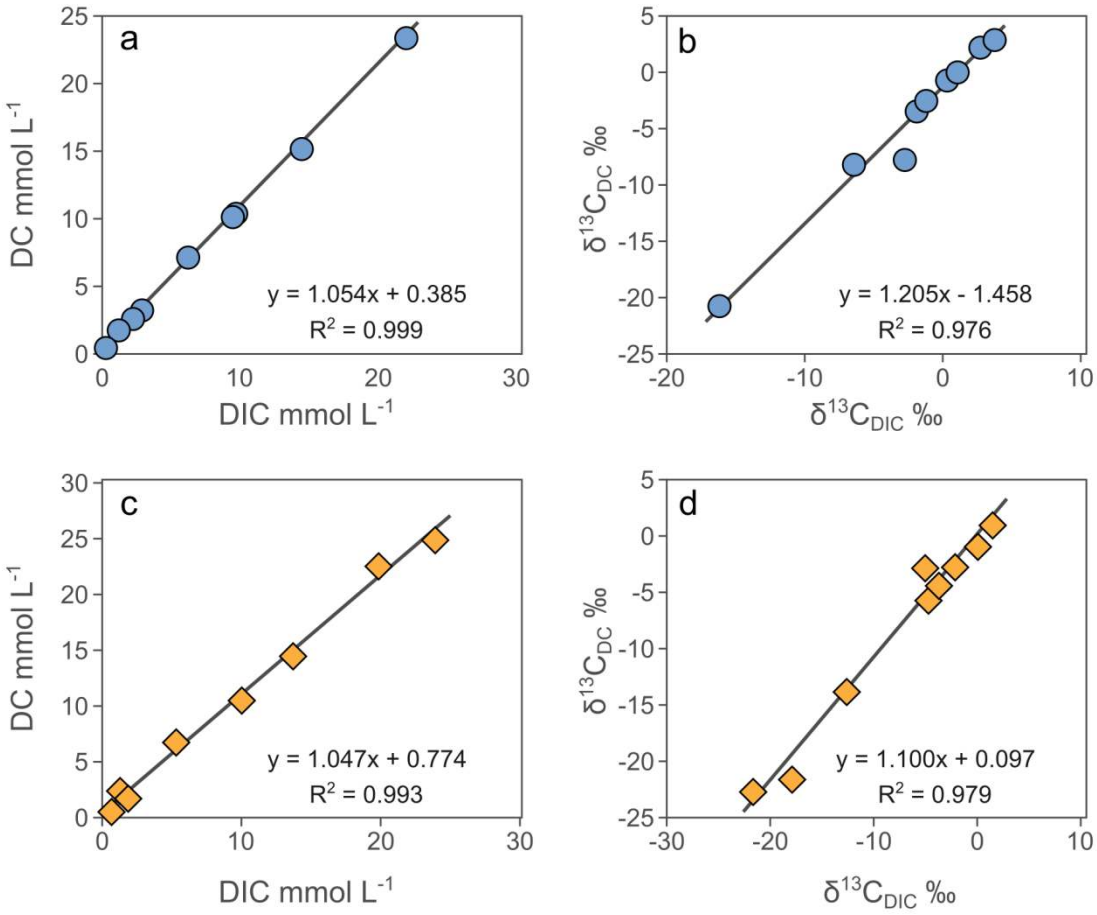

Extended Data Figure 3 – Relationship between DC and DIC concentrations and $\delta^{13}C$. Values for northern Costa Rica (panels A and B) are shown with blue symbols and central Costa Rica (panels c and d), with red symbols. Strong correlations allow prediction of DC concentrations and $\delta^{13}C$ values for the sites for which DIC compositions are lacking. The slope of the concentration plots is used to calculate the fraction of DIC and DOC in the sample suites.